Eddies and Currents in the Bay of Bengal during Summer Monsoons

A. Pirro[a,*], H. J. S. Fernando[a,d], H. W. Wijesekera[b], T. G. Jensen[b], L. R. Centurioni[c], S.U.P. Jinadasa[e,f]

[a]*University of Notre Dame, Department of Civil Engineering, Environmental and Earth Sciences, Notre Dame, IN 46556, USA*

[b]*Naval Research Laboratory, Stennis Space Center, MS 39529, USA*

[c]*Scripps Institution of Oceanography, University of California, San Diego, La Jolla, CA, USA*

[d]*University of Notre Dame, Department of Aerospace and Mechanical Engineering, Notre Dame, IN 46556, USA*

[e]*Ocean University, Mattakuliya, Colombo, Sri Lanka*

[f]*National Aquatic Resources Research and Development Agency, Colombo, Sri Lanka.*

Keywords: Anticyclonic eddy, Sri Lanka Dome, Bay of Bengal, Southwest Monsoon Current, Rossby waves, Laboratory experiment

Corresponding author.
E-mail address: apirro@inogs.it (A. Pirro)

ABSTRACT

The Southwest Monsoon Current (SMC) in the Bay of Bengal (BoB) and prominent eddies surrounding it, in particular, an anticyclonic eddy (AE) to the southeast and a cyclonic eddy (Sri Lanka Dome, SLD) to the east of Sri Lanka, were investigated using field observations, numerical simulations, satellite imagery, laboratory experiments and theoretical studies. The field campaigns were conducted in 2015 and 2018, respectively, in conjunction with the Air-Sea Interactions in the Northern Indian Ocean (ASIRI) and Monsoon Intra-Seasonal Oscillations in Bay of Bengal (MISO-BoB) research initiatives. Ship observations confirmed the presence of a annually recurring AE about 500 km southeast of Sri Lanka, with surface velocities up to ~ 1 m s^{-1}, size in the meridional direction ~ 200 km, and penetration approximately to the depth of the thermocline ~ 150 m. Satellite observations and COAMPS® model simulations show that the AE and the SLD are formed following the appearance of the SMC in early summer, and both evolve during July/August and disappear in September. This result is at odds with the prevailing notion that the AE is a result of the interaction between the SMC and Rossby waves arriving from the southeast of the BoB, carrying energy of a blocked Wyrtki jet at the Sumatra coast; such waves do not arrive in the southwestern BoB until August/September. Simultaneous appearance of AE and SLD is inconsistent with a recently proposed mechanism in which SLD is formed due to separation of the SMC from the Sri Lanka coast. A new hypothesis is proposed wherein the AE and the SLD are generated by topographically trapped Rossby wave response of the SMC to perturbations by the Sri Lankan coast. Observations of the size, location and origins of the AE were broadly consistent with this hypothesis, so were the results of a laboratory experiment designed to mimic natural flow in the BoB by creating an eastward jet (SMC) on a simulated β plane. Sea surface temperature (SST) observations show that the SMC carries colder upwelled

59 water from the southern Sri Lankan and Indian coasts and distributes it within the surface waters
60 of the AE and beyond. Thus, the surface waters of the AE are colder than that of the SLD,
61 notwithstanding perceived local upwelling in the SLD, suggesting that SMC may play a
62 controlling role in the air-sea interactions of the southern BoB.
63
64
65

1. Introduction

Monsoon-induced ocean currents play a key role in exchanging water masses between the Arabian Sea (AS) and Bay of Bengal (BoB). During northeast monsoons (December to April), fresher surface water from the BoB flows into AS via Northeast Monsoon Current (NMC) while during boreal summer (June to October) the Southwest Monsoon Current (SMC) transports saltier AS surface water to the BoB (Tomczak and Godfrey, 2003). The drivers of monsoonal currents and hence AS-BoB water exchange mechanisms are complex, and depend on the seasonal wind variability, shallow water ocean dynamics, bathymetry and land mass distribution. The monsoon currents reverse in the spring (April - May, NMC to SMC) and fall (October - November, SMC to NMC), leading to a myriad of phenomena that cover a swath of space-time scales (Shankar et al., 2002). Substantial understanding has been gained on monsoon currents and their transitions in the Indian Ocean (IO) using a variety of tools: regional circulation modeling (Vinayachandran and Yamagata, 1998; Das et al., 2016; Jensen 2001, 2003; Jensen et al., 2016); satellites, floats, drifters, and moorings (Murty et al., 1992; Schott et al., 1994; Shetye et al., 1996; McCreary et al., 1996; Schott and McCreary, 2001; Durand et al., 2009; Vinayachandran et al., 2013; Mukherjee et al., 2014; Wijesekera et al. 2016a, among the others); and research cruises (Wijesekera et al., 2015, 2016a,b; Mahadevan et al., 2016; Vinayachandran et al., 2018). Accordingly, the summer ocean circulation in BoB, away from the freshwater input areas, is mainly driven by the wind stress (Hastenrath and Greiscahr, 1991), with landmass distribution and shallow flow dynamics exerting a controlling influence.

During the summer, the West Indian Coastal Current (WICC) in the eastern AS flows southward (Shetye et al., 1990) whereas the East Indian Coastal Current (EICC) in the western BoB is generally northward at low latitudes (Rao et al., 1998); Fig. 1. Connecting AS and BoB is

90 the SMC, which is supplied mainly by low-latitude AS water west of Sri Lanka rather than by
91 WICC (Hastenrath and Greiscahr, 1991), and thus the SMC appears as an extension of the
92 Somali Current. During the initiation of southwest monsoons, the SMC flows around Sri Lanka
93 and forms a northeastward shallow flow, but as the summer progresses the SMC's origin moves
94 farther westward and it nominally flows eastward as an intense narrow zonal jet
95 (Vinayachandran et al., 1999). Shipboard and moored observations in the summer of 1991 by
96 Schott et al. (1994) has revealed that the SMC is confined to the upper ~ 100 m with eastward
97 transports of ~ 8 Sv between 5°39'N and 4°11'N along 80° 30'E. Wijesekera et al. (2016a)
98 estimated an averaged northward transport of ~ 8 Sv east of Sri Lanka near 8°N along a 100 km
99 wide current. Webber et al. (2018) estimated a northward transport across the east-west section
100 (85°30' – 88°30'E) along 8°N as 16.7 - 24.5 Sv.

101 Two eddy-like surface features of intraseasonal space-timescales are summer fixtures of
102 the southwestern BoB. One is a large anticyclonic eddy (AE) to the southeast of Sri Lanka, and
103 the other is an adjacent cyclonic eddy known as the Sri Lanka Dome (SLD) to the east of Sri
104 Lanka (Fig. 1). The cyclonic circulation in the SLD causes upward doming of the thermocline,
105 with potential of generating surface chlorophyll signatures due to upwelling (Vinayachandran
106 and Yamagata, 1998). The SLD has a diameter of ~ 200 – 300 km and is constricted between
107 eastern Sri Lanka and BoB. Conversely, the thermocline in the AE downwells and, being
108 unconfined, the AE is larger and elongated zonally. Long term mooring observations of
109 Wijesekera et al. (2016a, their Fig. 15c) indicate that the AE and the SLD are generally located
110 on either side of the SMC, with upwelling/downwelling as large as 3 - 4 m per day.
111

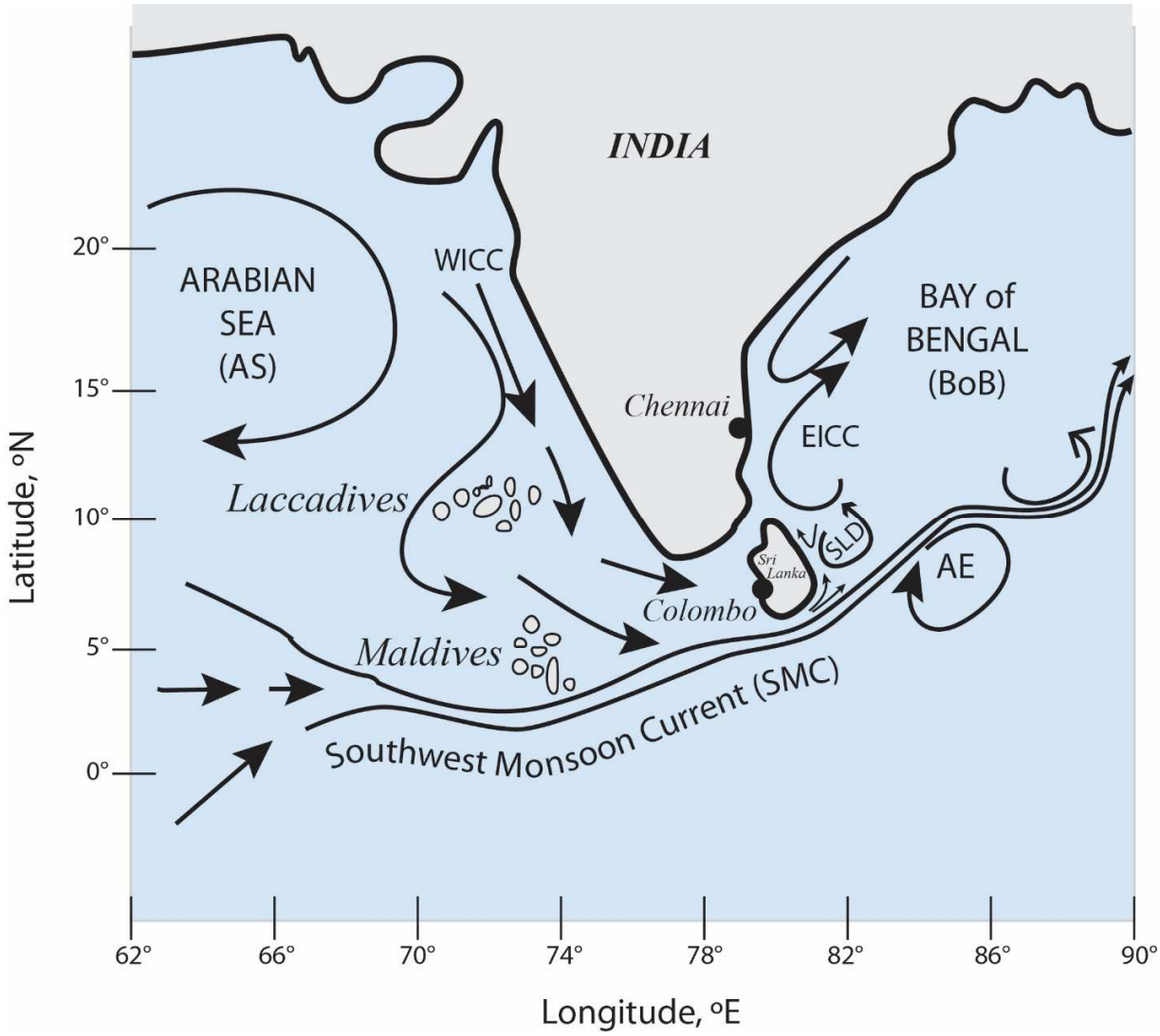

Fig. 1: A schematic of surface currents in the Northern Indian Ocean during the Summer Monsoon season.

Several hypotheses have been suggested for SLD formation. The first is the cyclonic wind stress-curl over southwestern BoB (McCreary at al., 1996; Vinayachandran and Yamagata, 1998; Schott et al., 2001). In the second, de Vos et al. (2014) argued that the separation of SMC from the (southern) boundary of Sri Lanka may lead to SLD. Accordingly, where coastal shelf friction is felt, the flow acquires a cyclonic (anticlockwise) relative vorticity (ω), gaining a

121 tendency to turn northward and leading to the SLD. De Vos et al. (2014) extrapolated the
122 numerical results of Alaee et al. (2004) and conducted their own numerical simulations using the
123 ROMS model. Simulations with and without Sri Lanka suggested that flow separation can be a
124 possible mechanism for SLD. Curiously, in some of their simulations, the SLD was not evident
125 (e.g. their Fig. 16 a,b) for flow parameters characteristic of BoB (velocity U ~ 0.2 – 0. 4 m s^{-1}).
126 None of the simulations captured the AE (their Figs. 2, 4).

127 A mechanism for the AE formation has been proposed by Vinayachandran and Yamagata
128 (1998), where the interaction of the SMC with Rossby waves arriving from the Sumatran coast
129 leads to the AE. In their simulations, a large AE connected with the SMC was formed during
130 geostrophic adjustment of BoB surface water converged by this interaction. The oncoming
131 Rossby waves carried substantial energy from the (equatorial) Wyrtki Jet that impinged on the
132 Sumatra coast in the late spring (Greatbatch, 1985; McCreary et al., 1993; Vinayachandran and
133 Yamagata 1998; Schott and McCreary, 2001). The conversion of mean kinetic energy to eddy
134 kinetic energy was evident, pointing to the involvement of barotropic instability in the AE
135 formation. Vinayachandran et al. (1998) found that the AE appears first in June, matures into a
136 near-circular shape in July, and then deforms in August.

137 The purpose of this paper is to (i) report the presence, location and properties of the AE
138 and the SLD during 2015 and 2018 field campaigns, supported by satellite products and
139 COAMPS® model output, (ii) to provide evidence that AE and SLD are formed simultaneously
140 surrounding the SMC in the early summer, and thus previous notions of their genesis (Rossby
141 waves arriving from the Sumatra coast or flow separation from Sri Lanka) need to be revisited,
142 (iii) to advance an alternative hypothesis for AE and SLD formation based on topographically
143 trapped Rossby wave generation associated with SMC and its barotropic instability, and (iv)

144 provide evidence for the new hypothesis using satellite products, COAMPS® simulations, and a
145 laboratory experiment.

146 The paper is organized as follows: in Section 2, we will discuss the drawbacks of existing
147 hypotheses on the formation of the SLD and the AE, and propose an alternative hypothesis.
148 Different tools used in our study, including measurements from two research cruises, satellite
149 platforms, numerical modeling and laboratory experiments, are discussed in Section 3. Ship-
150 based observations are given in Section 4 followed by, in Section 5, the results of numerical
151 simulations and satellite imagery analysis employed to obtain details over a larger spatio-
152 temporal swath of BoB. The results of a laboratory experiment designed to mimic the SMC
153 while achieving dynamic similitude (i.e. matched relevant non-dimensional parameters) are
154 given in Section 6, which allowed investigations under controlled conditions and test the new
155 hypothesis. Conclusions are given in Section 7.

156

157

158 **2. An alternative hypothesis for the formation of the AE and SLD**

159

160 Although the separation of the SMC from the Sri Lanka southern coast may produce
161 cyclonic vorticity that may be responsible for the SLD as argued by de Vos et al. (2014), such a
162 mechanism cannot produce negative vorticity for the genesis of the AE. Local wind stress curl
163 can be a factor for cyclonic circulation and upwelling in the SLD (McCreary at al., 1996), but
164 sustained presence over the summer and evolution of the SLD have not been correlated with
165 wind forcing. An alternative hypothesis proposed here is that perturbations to the eastward SMC
166 by Sri Lanka may trigger topographically trapped Rossby waves that undergo barotropic

instability, leading to both cyclonic (SLD) and anticyclonic (AE) eddies on the either side of the SMC (e.g. Fig. 1). The basic mechanism is that as the SMC flows northeastward, it is perturbed by the southern coastal topography of Sri Lanka, encounters an increase of planetary vorticity f, which can be quantified by the β plane approximation $f = f_0 + \beta y$, where y is the meridional distance and f_0 the reference planetary vorticity. The conservation of potential vorticity Π in shallow flows requires

$$\Pi = (\omega + f)/H = \text{constant} \tag{2.1}$$

where ω is the vertical relative vorticity and H the depth of the flow. If, for simplicity, the unperturbed flow is considered as uniform with negligible ω and the flow is assumed to be of uniform depth H_0, then (2.1) becomes

$$\frac{\omega+f_o+\beta y}{H_o} = \frac{f_o}{H_o}, \text{ or } \omega + \beta y \approx 0. \tag{2.2}$$

The assumption of constant depth H_o is a reasonable assumption for the SMC, as it is confined to a layer aloft the thermocline ($H_o \sim 150\ m$). As the northern extent of SMC increases, the relative vorticity ω needs to decrease, becomes anticyclonic ($\omega < 0$), and turns southward. This north-south meridional deflection recurs as the SMC flows eastward, signifying a barotropic Rossby wave (Batchelor, 1967, p. 577) and a meandering SMC. The barotropic instability of the meander may produce eddies on either side of it, as observed in the SMC east of Sri Lanka. The cyclonic eddy close to Sri Lanka can be identified as the SLD and the anticyclonic eddy as the AE. Modeling studies (Potemra et al., 1991; Yu et al., 1991; McCreary et al., 1993, 1996; Vinayachandran et al., 1996, 1999) are broadly consistent with the above depiction, although details and interpretations vary.

The general case of trapped Rossby waves in an approximately zonal mean flow $\overline{U}$(y) can be investigated using the linearized form of (2.1). The vertical vorticity ω can be written in terms of the mean $\bar{\omega}$ and perturbation vorticity, $\omega = \bar{\omega} + \omega'$, $\bar{\omega}=-\partial\overline{U}/\partial y$, leading to

$$\left(\frac{\partial}{\partial t} + \overline{U}\frac{\partial}{\partial x}\right)\omega' + v'\frac{\partial}{\partial y}(\bar{\omega} + f) = 0, \tag{2.3}$$

where v' is the meridional velocity fluctuation. Introducing the stream functions $u'=\frac{\partial\psi}{\partial y}$ and $v'=-\frac{\partial\psi}{\partial x}$, (2.3) becomes

$$\left(\frac{\partial}{\partial t} + \overline{U}\frac{\partial}{\partial x}\right)\nabla^2\psi + \frac{\partial\psi}{\partial y}\frac{\partial}{\partial y}(\bar{\omega} + f) = 0. \tag{2.4}$$

If $\overline{U} = U_0$ (or $\bar{\omega} = 0$) for simplicity, for trapped (non-propagating) waves of the form $\psi = \psi_o e^{i(kx+my)}$, (2.4) on the β plane gives $\kappa=(\beta/\overline{U}_o)^{1/2}$, where $\kappa^2 = k^2 + m^2$. The wavelength of the Rossby-wave becomes $\lambda=2\pi(\overline{U}_o/\beta)^{1/2}$. According to Gill (1974), such waves are unstable and produce anticyclonic and cyclonic eddies (of the genre of AE and SLD), supporting our hypothesis. Initially the amplitude of the instability wave is on the order shear layer thickness (~ 150 km), and thus the generated eddies takes an elliptical form. They evolve into a more circular shape with time.

Accordingly, for the SMC, λ ~ 1000 km (β = 2.2 10^{-11} m^{-1} s^{-1}, U_0~ 0.7 m s^{-1}), and an anticyclonic eddy is expected to appear $\pi(U_0/\beta)^{1/2}$ ~ 500 km east of the southern coast of Sri Lanka, which approximately matches with observations to be described in Section 4. A zonal flow subject to a constant Coriolis parameter (i.e. f plane, β = 0) may also undergo barotropic instabilities. In this case, the instability wave-length is ~ $2.5(2\pi L)$ km (Gill 1982, p. 567), where L is the width of the current. For the SMC with L ~ 150 km (Shetye et al., 1990), half of the wave-length is about 1200 km, which is much larger than typical observations, suggesting the

importance of β plane dynamics. In all, the above calculations support the notion that the AE and the SLD may be due to instabilities of topographically trapped Rossby waves.

3. Methods

3.1. Field Measurements

The field data were collected in the summers of 2015 and 2018, in conjunction with the cruises of the US Office of Naval Research's (ONR) initiatives on Air-Sea Interactions in Northern Indian Ocean (ASIRI, 2012 – 2017; Wijesekera et al., 2016a,b) and Monsoon Intra-Seasonal Oscillations in Bay of Bengal (MISO-BoB, 2017–2022). ASIRI focused on the role of upper ocean processes in monsoon dynamics, and MISO-BoB on sub-seasonal scale air-sea interaction phenomena and their role in monsoon variability.

The summer 2015 cruise (August 1 to August 15) was conducted aboard the R/V Roger Revelle and the 2018 cruise (June 30 to July 21) on R/V Tommy G. Thompson, both operated out of Colombo, Sri Lanka. In 2015, six deep-ocean moorings deployed in a December 2013 cruise were recovered; see Wijesekera et al., (2016a). The winds during the 2015 cruise were consistently southwesterly, from 1.7 to 19.5 m s^{-1} (Fig. 2). The zonal and meridional components of the horizontal current vector were measured along the cruise track using a ship-mounted 150 kHz Acoustic Current Doppler Profiler (ADCP). The shipboard Conductivity, Temperature, and Depth (CTD) profiler (Seabird; 24 Hz sampling rate) was deployed for 24 h at 85.21°E - 6.42°N on August 11 – 12 2015 (yellow square in Fig. 2 or black square in Fig. 4), with casts

taken every 30 minutes down to 250 m and the data binned over 5 m depth intervals. In addition, drifter observations from 2012 to 2015 conducted as a part of ASIRI were available, and we have used Surface Velocity Program (SVP) drifters (Centurioni, 2018) designed to measure ocean currents at 15 m depth with accuracy better than 10^{-2} m s^{-1} for wind speed up to 10 m s^{-1} (Niiler et al., 1995). The drogue depth of 15 m ensures that the direct (i.e. Stokes Drift) and spurious (e.g. rectification) effects of surface waves are small and the measurements represent ocean currents in the mixed layer.

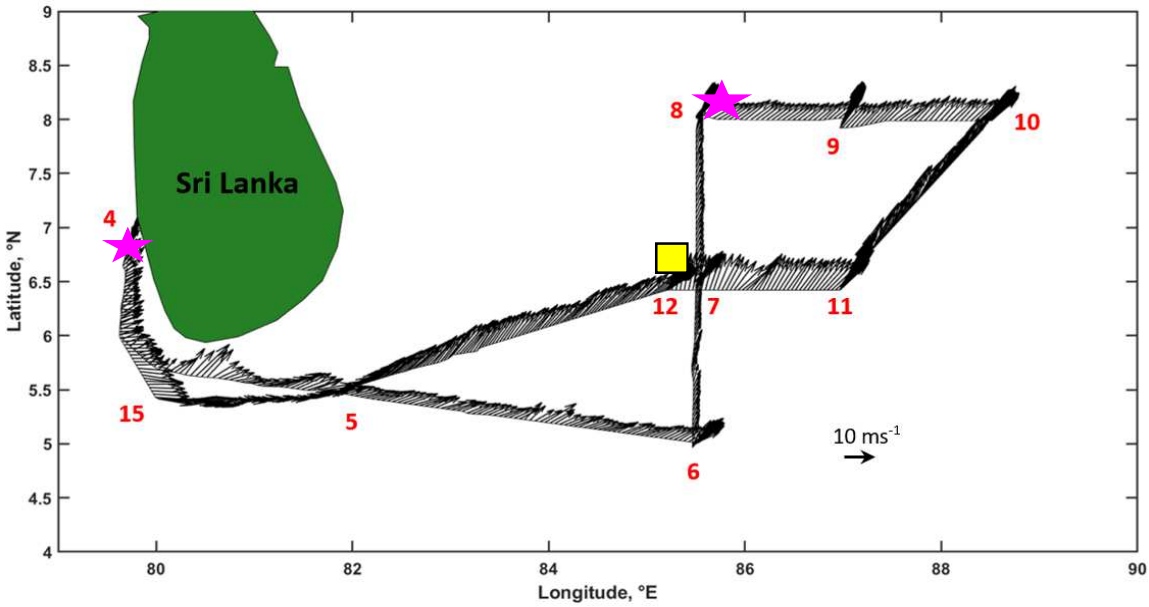

Fig. 1: Wind vectors along the ship track measured on the ship's meteorological mast. In red the day of August 2015. Magenta stars indicate drifter release points for 2015. Yellow square is the 24-hour CTD station

The 2018 deployment included atmospheric and air-sea measurement systems, but here the focus is on those relevant to the present study. Besides the shipboard ADCP measurements,

CTD casts were taken along the ship track (Seabird profiler; 24 Hz sampling rate and 5-m bin size) for the entire cruise period, unlike in 2015. Surface currents were tracked using seven SVP drifters deployed inside the SLD (8°N, 83.75°E) on July 15 while the sea surface temperature (SST) along the ship track was sampled using a Remote Ocean Sensing Radiometer (ROSR; http://rmrco.com/). Meteorological instruments were mounted on the ship's bow mast (flux tower). A sonic anemometer at 16 m measured the fluxes of momentum and heat; and a LI-COR® open path infrared gas analyzer measured moisture and latent heat fluxes at 12 m. Moisture and temperature profiles were sampled by the microwave radiometer.

3.2 . Auxiliary Data Products

The daily Sea Surface Height Anomalies (SSHA) data from Archiving, Validation and Interpretation of Satellite Oceanographic (AVISO) with 0.25° spatial resolution (ftp://eddy.colorado.edu) were averaged over the 2015 cruise period as well as for the month of July 2018. The daily Optimum Interpolation Sea Surface Temperature (OISST) data of NOAA's National Center for Environmental Information (NCEI) with a spatial resolution of 0.25° and daily NOAA Outgoing Longwave Radiation (OLR) with 1° spatial resolution were used to obtain further information. Simulations of the Coupled Ocean/Atmosphere Mesoscale Prediction System (COAMPS®) were also used to support the data analysis. The model provided velocity, temperature and salinity structure of the region for the 2015 cruise period; see Jensen et al., (2015) for modeling details.

3.3. Laboratory Experiments

271

272 To investigate the role of the β effect (topographic Rossby waves) in generating AE and
273 SLD due to interaction of SMC with Sri Lankan coast, a laboratory experiment was conducted in
274 a water tank placed on a rotating table. The β effect was simulated using an adjustable sloping
275 bottom, and a jet flow (representing the SMC) was directed at a scaled model of Sri Lanka (see
276 below). The experimental design involved satisfying dynamical similitude to the extent possible;
277 that is to match the crucial non-dimensional parameters between the nature and laboratory, which
278 could be obtained by non-dimensionalizing the reduced potential vorticity equation (2.2) using
279 characteristic length L_0 and velocity U_0 scales, viz.,

$$\omega^* + \frac{\beta L_o^2}{U_o} y^* = 0, \quad \omega^* = \nabla \times u^*, \tag{3.1}$$

280 where $u^* = u/U_o, y^* = y/L_o$. Thus, disregarding the molecular viscosity ν, the critical
281 dimensionless parameter for modeling the SMC and its spatial evolution in the laboratory is

$$\pi = \frac{\beta L_o^2}{U_0}. \tag{3.2}$$

282 Upon generation, the evolution of eddies due to instabilities is governed by the local
283 Coriolis parameter f, and thus the Rossby number $Ro = U_0/fL_0$ (<<1) becomes important as an
284 additional parameter. In our case, however, the main focus would be the formation of
285 topographically trapped eddies downstream of Sri Lanka, although Ro was kept low to satisfy
286 the Rossby number criterion.

287 It is not simple to simulate actual the β effect (or spatially varying f) on a laboratory
288 rotating table. To this end, Boyer and Davies (1982), among others, have cleverly simulated the
289 β effect in a laboratory water tank using a sloping bottom topography of inclination α, with the

water depth h linearly reducing northward with (meridional) distance y as $h = h_0 - \alpha y$. For barotropic flows, the slope angle α was shown to be dynamically equivalent to the β (effect) according to

$$\beta = \frac{f_0\,\alpha}{h_o}, \tag{3.3}$$

which was used in our experimental design. Boyer and Davies (1982) also showed that viscous effects, signified by the Ekman number $Ek = \nu/f_0 L^2$, are negligible for $Ek << 1$.

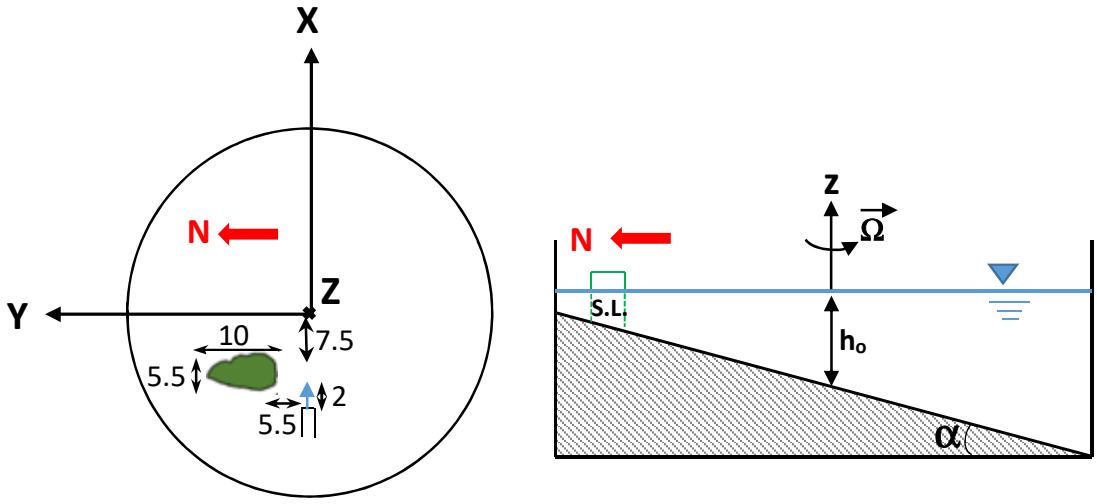

Fig. 3: Top view (left) and side view (right) of the laboratory experiment set up. Red arrow and Ω indicate the north direction and the angular velocity of the tank, respectively. The green area represents the Sri Lanka. The bottom slope is α and the water depth at the center is h_o. Units are in cm.

Fig. 3 shows a schematic of the laboratory set up. The experiments were carried out in a round Plexiglas tank of diameter 80 cm, located within another water-filled square box to minimize the optical distortions introduced when viewed from the sides. The tank was mounted on a rotating table that could operate at a constant speed Ω. The tank bottom was sloped to simulate the β effect, and the coordinate system (x, y, z) was selected with z vertically up, x

eastward and *y* northward. A solid model of Sri Lanka was introduced with a radial offset (~ 10 cm) from the center of the tank, and this selection (offset > $U_0/2\Omega$ ~ 6 cm) minimized the effects of streamline curvature on the jet flow. The jet was introduced to the southwest of Sri Lanka (~ 5 cm away) by a constant-flow-rate pump that drew water from an overhead tank. The jet was mixed with 100 - 350 μm fluorescent particles, which, when illuminated with an Argon-Ion laser sheet, produced clear trajectories of particle streaks that were tracked by an overhead mounted digital camera (0.36 Mpixel) looking downward. The camera, water reservoir and jet pump were all on the rotating platform. The trajectories of particle streaks were analyzed using the tracking software described in Hocut et al. (2015). Only the barotropic case was considered, given that the dynamical equivalence (3.3) is not valid for baroclinic cases.

The dynamic similarity requires matching of π. In nature, β = 2.2 x 10^{-11} m s^{-1}, U_0 ~ 1 m s^{-1} and L_0 = 225 km (the estimated size of perturbations – curvature of Sri Lanka's southern coast), and hence $\pi = \beta L_0^2/U_0 \approx 1.1$. This is consistent with the estimates of Boyer and Davies (1982) that for typical geophysical flows π ~ 1. In the experimental design, β in the laboratory was matched by its surrogate, the northward slope α, using $\beta = \alpha f_0/h_o$ ~ 0.01 cm s^{-1} (α ~ 2.5°, f_0 = 0.26 rad s^{-1} and h_o = 1.5 cm), and then the required velocity for laboratory flow was obtained as $U_o = \beta L_o/\pi$ ~ 1.3 cm s^{-1} with L_o = 12 cm. While it is appealing to cover a range of π, R_o and *Ek* such an effort deemed beyond the scope of this paper where the focus is π ~ 1, *Ek* << 1 and R_o < 1. Therefore, the selection was: U_0 = (1.3 - 1.7) cm s^{-1}, bottom slope α = (2.3° - 2.5°; the range of tolerances possible), the mean water depth h_0= 1.5 cm, f_0 = 0.26 rad s^{-1}, *Ro* ~ 0.3 – 0.5 and *Ek* ~ 4.2 10^{-3}. In the SMC, R_o varies between 0.3 and 0.5 for U_0 ~ 1 m s^{-1}, f_0 = 1.2 10^{-5} rad s^{-1} (latitude 5°N), L_0 = 225 km and *Ek* ~ 6.8 10^{-12}.

After ensuring that fluid in the tank and in the supply reservoir and the particles were all spun-up to solid body rotation, the pump introduced an eastward jet at the prescribed velocity. According to Killworth (1980), the inclination of the current to the zonal direction is unimportant for dynamics, when the inclination is small.

4. Observations of SMC and eddies

4.1. Observations during 2015 ASIRI cruise

Shipboard observations in August 2015 provide space-time sections of currents along the ship tracks. Velocity averaged over 5 m above and below the indicated depth are shown in Fig. 4. The uppermost layer indicates approximately eastward/southeastward flow along 5.62°N and from 80°E to 82°E of magnitude 0.5 - 0.7 m s^{-1}. Thereafter, the flow turns northeastward (82° - 84.6 °E, 5° - 6.25°N) while increasing the velocity up to ~ 1 m s^{-1}. According to Vinayachandran et al. (1999), a branch of the seasonal SMC flows eastward and another penetrates northeastward, and hence the signatures of the SMC could be traced at least up to 8°N and 85.5°E with an averaged surface velocity of ~ 0.7 m s^{-1}. (Note that currents measured during June 2014 has also shown strong eastward flow, where 15 min averaged velocity in the upper 175 m was as large as 0.8 m s^{-1}; Fig. 7 of Wijesekera et al., 2016b). Along the northern zonal transect (8°N, 85.5° - 88.5°E), the eastward flow gradually turns southwestward at approximately the mid-point of transect, pointing to a large AE. The radius of the AE estimated through its center along the meridional section is ~ 250 km, the zonal extent being larger. In the BoB the AE appears roughly at 500 km from the south coast of Sri Lanka, consistent with the theoretical estimates of Section 2.

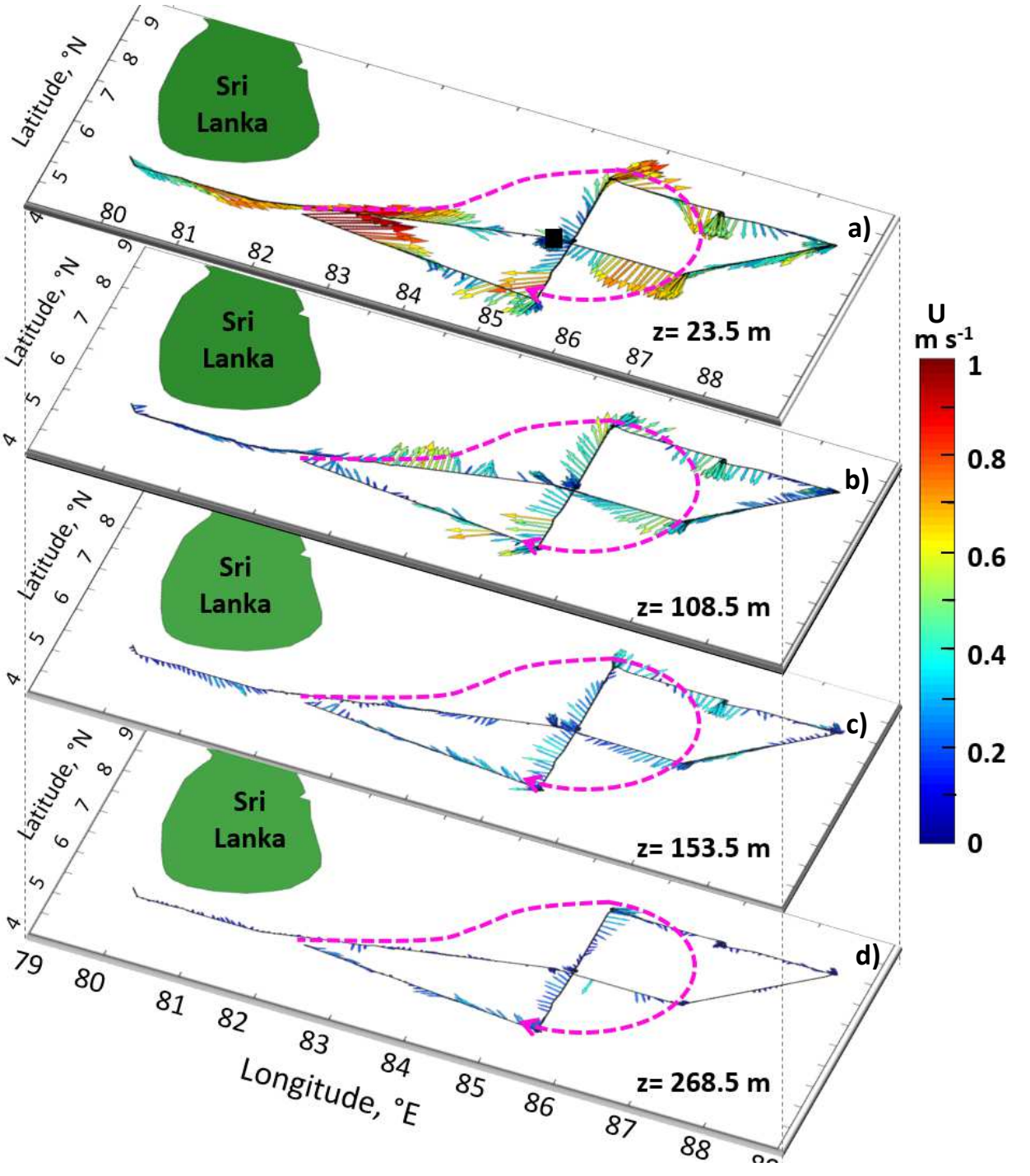

Fig. 2: ADCP velocity vectors along the cruise track during August 4 - 15 2015. Data from 5 m below and above the indicated depth are averaged over 30 minutes. Magenta broken lines indicate the AE based on isotachs of 0.8 m s^{-1}. The black square in the top panel indicates the CTD station.

In Fig. 4, the magenta broken line (approximate isotachs) identifies the AE. The velocity field in the AE gradually decreases downward and substantially decays below z ~ 150 m where a well-defined eddy could not be identified. The (T - S - σ_t) structure measured in the CTD sampling station (Fig. 2 and 4a) while the ship is nearly stationary is shown in Fig. 5. A strong thermocline is evident over ~ 80 m to 180 m. Water of elevated salinity possibly intruding from the AS to BoB in the depth range 60 – 90 m underneath the surface layer is evident, in agreement with previous climatological studies (e.g. Vinyachandran et al., 2013) and moored observations of Wijesekera et al. (2016a; their Fig. 3b) at 85.5°E - 6.5°N, where higher values of salinity (~ 36 psu) were recorded in conjunction with the northeastward flow.

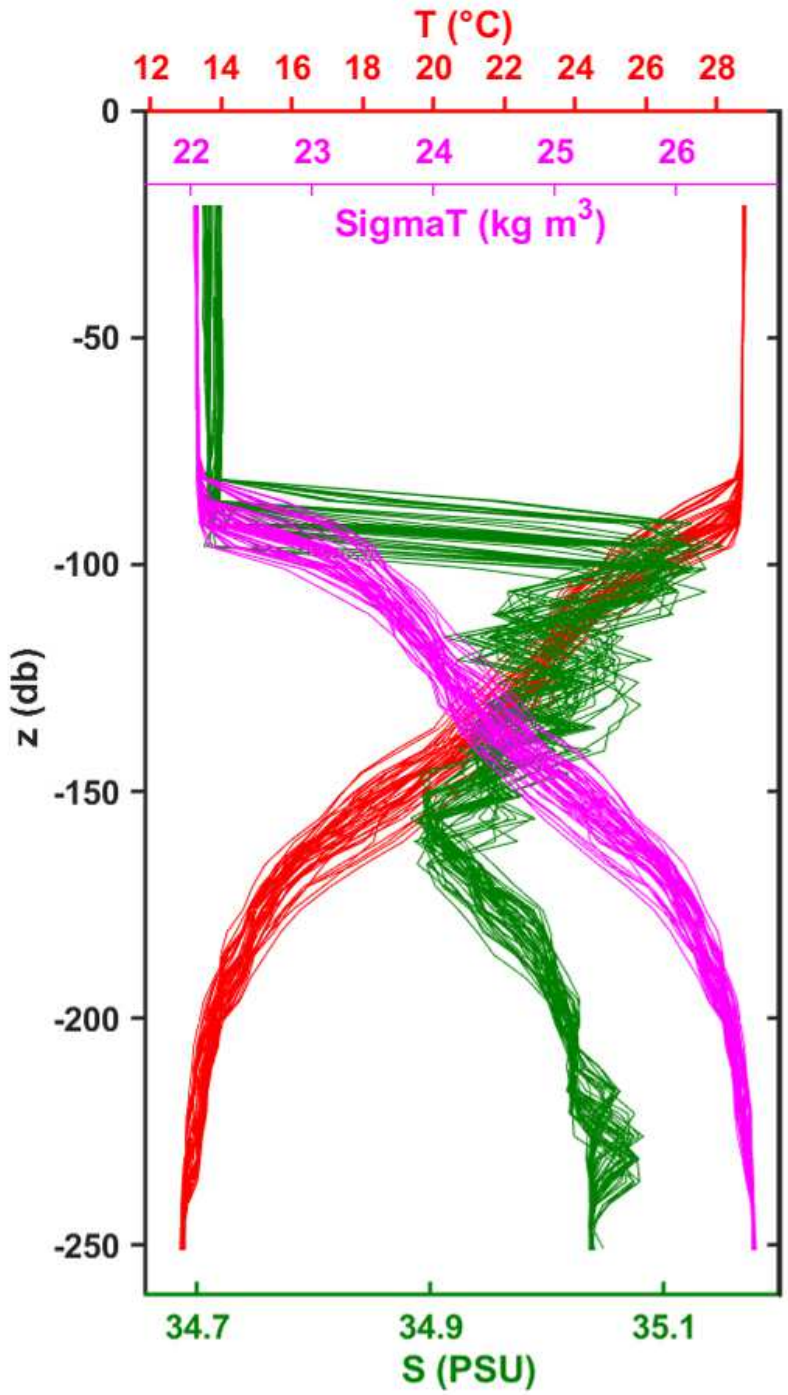

Fig. 3: CTD Temperature, Salinity and σ_t profiles collected at 85.21°E, 6.42°N on August 11-12 2015. Sampling location is indicated in Fig. 2a and Fig. 1.

Observations for August 1 - 15, 2015 are shown in Fig. 6. Panel (a) shows SSHA averaged over this period, overlaid by ADCP surface currents (averaged over upper 24 m) along the ship track, and 2015 drifter trajectories. The yellow area, particularly with 5 - 10 cm positive SSHA, identifies the anticyclonic mesoscale feature that extends over the moorings region. This overlaps with the AE inferred by current measurements (Fig. 4). The dark blue patch to the west of the AE (83° - 85°E, 8° - 10°N) is the SLD with negative SSHA between -20 and -10 cm. The trajectories of drifters released from August 1 to August 31, 2015 are identified by white dotted lines. One travelled northward along the Sri Lanka east coast and the others tracked the AE approximately. Specifically, white trajectories indicate a southwestward flow which delimited the outer borders of the AE. Trajectories of drifters released from July 16 to August 2 2014 during an earlier cruise (not discussed) tracked a southward flow associated with the SLD. We note that drifters released in 2012 and 2014 (not shown) also show similar behavior, indicating the seasonally recurring behavior of AE; see Fig. 1a of Lozovatsky et al. (2016) for SLD position in 2014).

Useful properties of the AE and the SLD are evident from SST in Fig. 6b. A warmer surface area (~ 29.4°- 29.8°C) occupies the area immediate east of Sri Lanka (82° - 82.63°E, 7° - 9°N) while a relatively colder surface temperature (~ 28.2° - 28.8°C) is observed in the region of the AE and its vicinity (83°- 89°E, 5° - 10°N). The SST imagery suggests that surface colder waters (~ 25.8° - 27.92°C) upwelled in the southern coasts of Sri Lanka and India, are advected to the southcentral part of BoB via the SMC while dispersing off horizontally by complex eddy structures. The surface waters of the SLD (see SSHA in panel a) are warmer, with temperatures as high as 29° - 29.8°C, indicating that local upwelling in the SLD is not as effective at this time in determining surface temperature. High OLR (> 220 W m^{-2}) observed during the observational

period indicated suppressed convection activities during the cruise period (not shown). In all, for the analysis period of 2015, it appears that colder water advection to the AE area may have implications on air-sea interactions by reducing SST and hence suppressing convective activity.

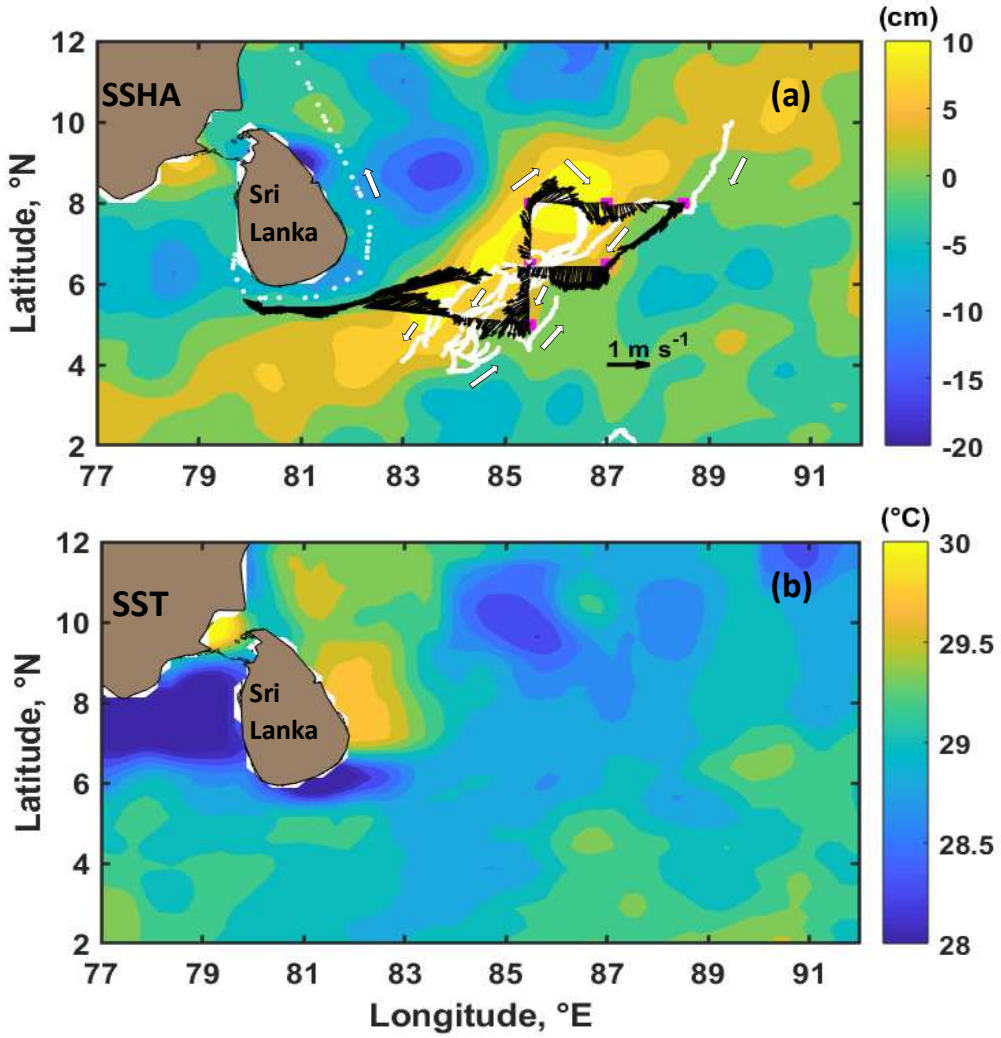

Fig. 4: Panel(a) represents the AVISO SSHA averaged values (August 1st-15th 2015). White drifter trajectories are from August 1st to 31st 2015, with arrows denoting drifters flow direction. Magenta squares and black arrows indicate, respectively, deep mooring locations and the ADCP averaged velocity vectors in the upper 24 m during the cruise period. Panel (b) show satellite Sea Surface Temperature (SST)

465

466

467 *4.2. Observations during 2018 MISO-BoB cruise*

468

469 The 2018 MISO-BoB cruise was designed to collect simultaneous oceanic and
470 atmospheric data. Observations of SSHA, SST and OLR (all July averaged), *in-situ* currents
471 measured by the shipboard ADCP, and drifter trajectories are all presented in Fig. 7. While one
472 on one comparison between climatological satellite maps and *in-situ* observations is not possible
473 because of space-time scale differences in measurements, they are overlaid for rough
474 comparisons. As in the 2015 case, the signatures of larger AE (magenta broken line) and SLD
475 (blue area northwest of AE) are still evident from the mosaic of SSHA, shipboard ADCP current
476 and drifter measurements (Fig. 7a). Drifters released within the SLD (yellow circle in Fig. 7a)
477 were entrained into the SMC and travelled toward the eastern BoB, however, some of the drifters
478 were encroached later into nearby cyclonic eddies at 10°N and 89°E (in red) and 93° - 95°E (in
479 magenta and yellow), indicating possible alternative cyclonic and anticyclonic structures
480 hypothesized in Section 2. The 10-minute averaged SST measured using ship's ROSR is overlaid
481 on a satellite SST climatology map in Fig. 7b, and the atmospheric surface temperature measured
482 by the bow mast (~16 m height, 10-minute averaged) along the ship track is superimposed on a
483 satellite-based OLR in Fig. 7c. The wind direction was southwesterly during this cruise period.
484 Latent and sensible heat fluxes (10-minute averaged) from the bow mast are shown in Fig. 7d.

As in 2015, coastally upwelled cold water is advected by the SMC into the southern BoB, the effect of which on the atmosphere is evident by the lower latent (104 Wm^{-2}) and sensible (-5.5 Wm^{-2}) turbulent heat fluxes along the ship track through the (upwelled and advected) colder water, compared to the heat fluxes (169 Wm^{-2} and 3 Wm^{-2}) in relatively warmer water to the north measured at 12:00 UTC (but on different days). The SST difference between most northern and southern points of the meridional ship track (85.45°E, 4° - 14°N) measured by ROSR is ~ 1^{o}C while the ship bow mast (~16 m height) shows an atmospheric surface temperature jump ~ 0.5^{o}C over the same distance (taken at 12:00 UTC). The OLR climatology (> 200 Wm^{-2}) indicates that southwestern BoB was devoid of high clouds and convective activity during the July 2018 (Fig. 7c), which is broadly consistent with the observed heat fluxes (that depend on the SST and atmospheric temperature).

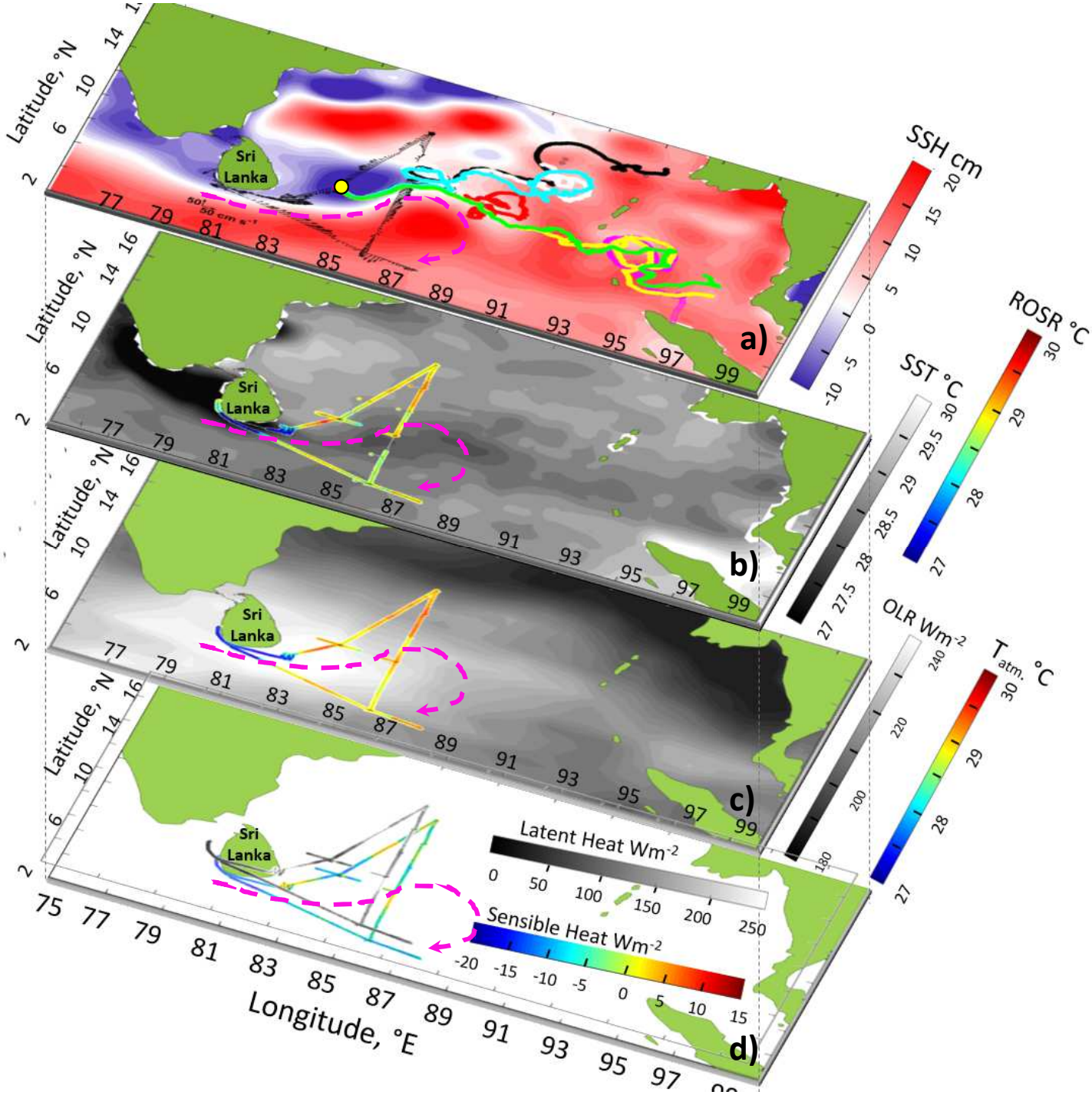

Fig. 5: Panel a: AVISO SSHA map averaged over July 2018. Black arrows represent ADCP velocity vectors along the ship track (June 30 - July 20 2018) averaged for the upper 60 m and every 45 minutes. Seven drifter's trajectories (July 15 – October 29) are indicated by the colored dots. Yellow circle represents their release point. Magenta broken line highlights the anticyclonic eddy location based on SSH). Panel (b): AVISO SST map averaged for July 2018 and ROSR SST along the ship track. Panel (c): NOAA OLR map averaged for July 2018 and atmospheric surface temperature from the bow mast (~ 16 m height) along the ship track. Panel (d): Latent and sensible heat fluxes from the bow mast (~ 16 m height) along the ship track

Twenty three CTD casts were made along the ship track, and here we report only the ones taken within the AE (Fig. 8a), at the border between two eddies (Fig. 8b) and inside the SLD (Fig. 8c). The data confirmed that the surface waters of the AE is colder than the SLD. Inside the AE (black circles in Fig. 8d and Fig. 8a), the mixed layer depth (MLD) was ~ 75 m with a nearly homogeneous temperature ~ 28.3°C (MLD was based on the 0.2°C criterion). On the northern periphery of the AE (green triangles in Fig. 8d and Fig. 8b) the MLD has decreased, reaching a depth of ~ 20 m while the averaged mixed-layer temperature increasing up to 28.6°C underlain by a shallower pycnocline (~140 m). As expected, the thermocline becomes shallower toward the SLD. Inside the SLD (magenta stars in Fig. 8d and Fig. 8c), the MLD slightly increased to ~ 35 m along with the surface temperature reaching ~ 29.2°C. This confirms that the mixed-layer temperature in SLD is (~ 0.9^{o}C) higher than that in AE, which is reflected in the SST.

In summary, a synthesis of R/V and satellite observations taken during the summers of 2015 and 2018 confirms the seasonal recurrence of the AE and SLD and their location on either side of the SMC. The surface temperature differences between the SLD (warmer) and the AE (colder) is due to the advection of upwelled colder water by the SMC, which also suppresses latent and sensible heat fluxes. Upwelling of colder water in SLD appears to be impeded by a strong thermocline. Southwestern BoB was devoid of convective activity compared to the northern part of the bay during the observations, as evident from OLR.

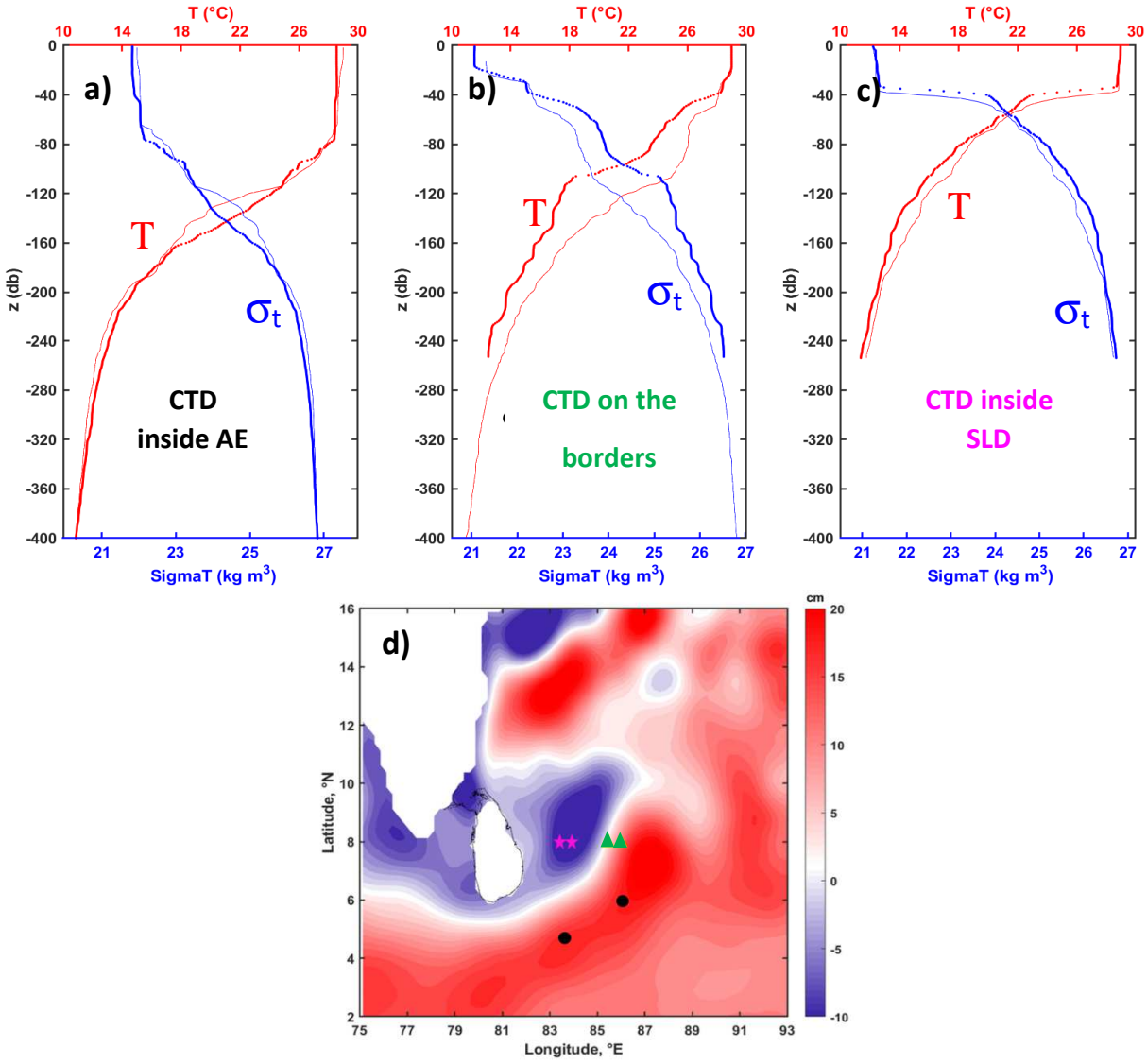

Fig. 6: Temperature (in red) and Sigma T (in blue) profiles (from CTD analysis) inside the AE (panel a), on the borders (panel b) and inside the SLD (panel c). CTD locations are indicated in panel d: black circles indicate CTD locations inside the AE, green triangles on the borders, and magenta stars inside the SLD. Map of SSHA (in cm) averaged for July 2018 is presented in panel d.

5. COAMPS® model output and AVISO SSHA data

A snapshot of the velocity field in the upper 25 m layer for August 25, 2015 based on COAMPS® simulations is shown in Fig. 9. A strong jet-like current ~ 1 m s^{-1} is present south of Sri Lanka. With its origin at ~ (75°E, - 5°N), this northeastward current is perturbed as it flows past the southern coast of Sri Lanka and folds into a strong anticyclonic circulation, evolving into a meander sandwiched between anticyclonic and cyclonic eddies. The signature of the AE was detected up to a depth ~ 150 m, and vanished for depths > 200 m (not shown). Specifically, the head of the eddy (~ 84° - 87.5°E, 6° – 10°N) had a velocity of about 0.5 m s^{-1} while the tail (~ 78° - 84°E, 4° – 6°N) registered weaker velocities of ~ 0.14 m s^{-1}. These results are in general agreement with the ADCP data showed in Fig. 4. Also evident is a weaker current (~ 0.5 m s^{-1}) from the north of BoB (magenta circle) that entrains into the anticyclonic eddy. The presence of such southward flow with the same order of magnitude is evident in ROMS simulations described in de Vos et al. (2014) and was evident in 2014 drifter data (not shown). The outer eastern border of the AE tracked by the white drifters (Fig. 6a) in the area 83° – 87°E, 4 – 8°N, is also captured by COAMPS® velocities ~ 1 m s^{-1}. Also, the general structure simulated SMC shows its meandering around anticyclonic and cyclonic eddies. The first cyclonic eddy (SLD) is distorted by the presence of the Sri Lanka landmass. Killworth (1980) has pointed out that instabilities of planetary waves can be strongly modified by side and bottom boundaries, and we expect a similar complex flow situation here.

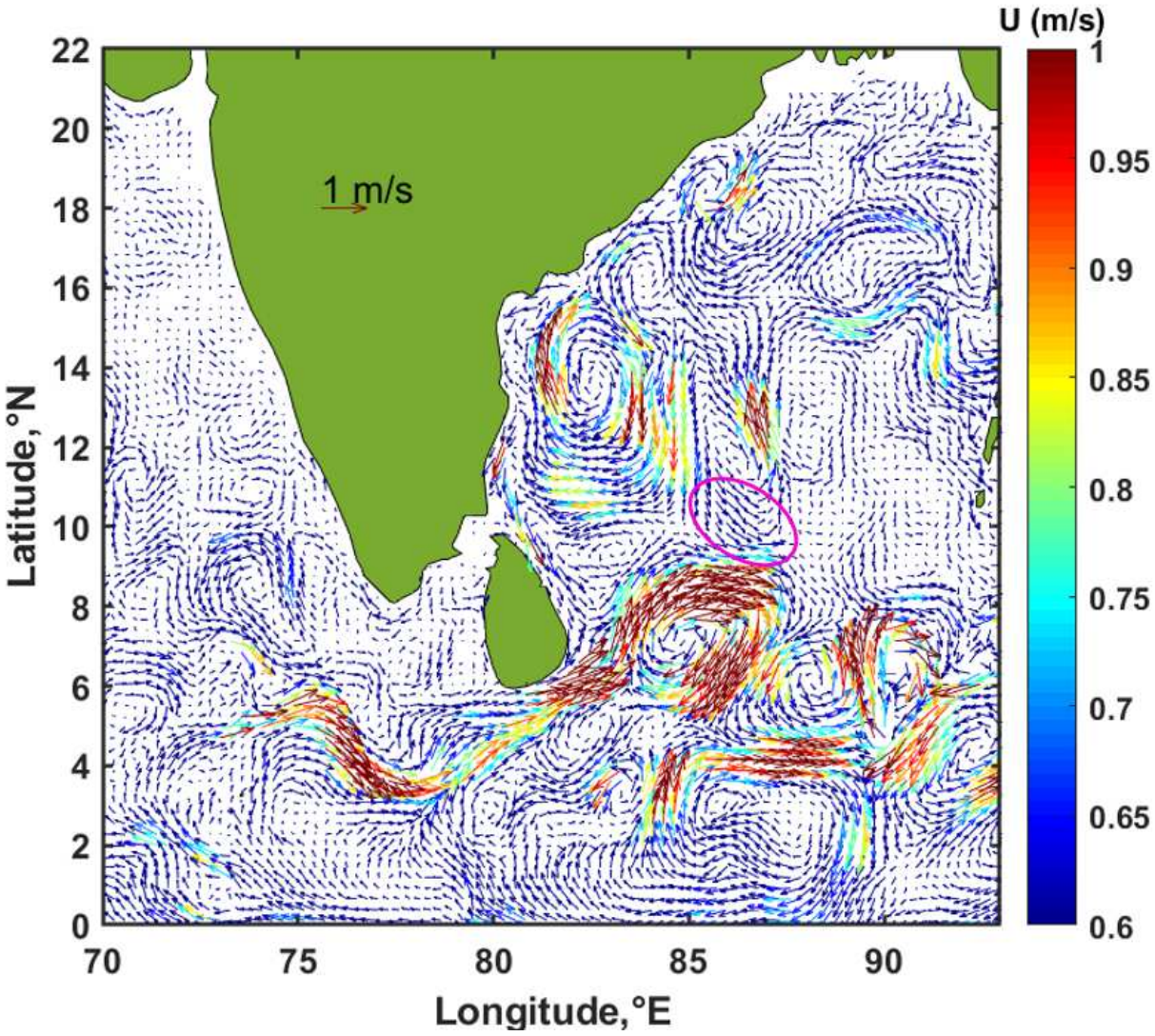

Fig. 7: Velocity field snapshot from COAMPS® model for August 25th 2015. Currents vectors are averaged over the upper 25 m depth (and every three hours).

585

586 To investigate the proposal of Vinayachandran and Yamagata (1998) that the arrival of
587 Rossby waves generated off the coast of Sumatra due to impingement of a spring Wyrtki jet may
588 be a cause for the AE formation, an animation of daily (AVISO) SSHA was constructed (see,
589 supplementary material). It covered the region (70° - 100°E, 5°S - 24°N) for May 1, 2015 to
590 December 31, 2015, which included the entire summer monsoon and a part of the winter
591 monsoon. Six snapshots of this animation clearly show that the AE is originated alongside the
592 SMC (Fig. 10 b,c), simultaneous with the SLD, before the expected arrival of Rossby waves
593 from southeast in August/September. The SLD is evident from June to August (black ellipse); it
594 originated in early June north of the developing AE (magenta ellipse), was fully developed by
595 the middle of June, slowly pushed westward toward the end of August, and faded away by
596 September. Most probably the AE, a high-pressure center, ensures the northward movement of
597 the SLD, which is a low-pressure system. A similar evolution of the SLD has been noted during
598 the 2014 summer Monsoon (Lozovatsky et al., 2016; Wijesekera et al., 2016a).
599 Positive SSHA (~ 5 - 20 cm) recorded in the area (80° - 86°E, 2° - 5°N) in early June,
600 2015 (Fig. 10b) confirms that the AE was generated following the initiation of the SMC around
601 April 26, 2015, identified based on the shift of the wind direction. The anti-cyclonic vortex is
602 slowly distorted up to 8°N, taking an elliptical shape with a northeast-southwest major axis in
603 August 2015 (Fig. 10 d,e), possibly due to the presence of continental boundaries. The AE
604 intensified at the beginning of September (Fig. 10f), reaching SSHA > 20 cm while becoming
605 more circular due to distortion. These observations point to a possible contribution of Rossby
606 waves arriving from the southeast to the evolution of the AE after August/September. In fact,
607 Wyrtki (1973) showed that accumulation of water off Sumatra in May disperses slowly during
608 the following two months. A time - longitude section of meridional velocity along 8°N

constructed from the modeling results of Vinayachandra et al. (1998; their Fig. 9) also confirms that Rossby waves from the southeast do not arrive at the southwestern BoB until September. Similar SSHA analyses were conducted for prior years (2010-2014), and the animations confirmed the formation of AE almost simultaneously with the SLD at the beginning of June, following the genesis of SMC (not shown). Thereafter, eddies develop in July-August and disappear in September, providing support for the hypothesis proposed in Section 2.

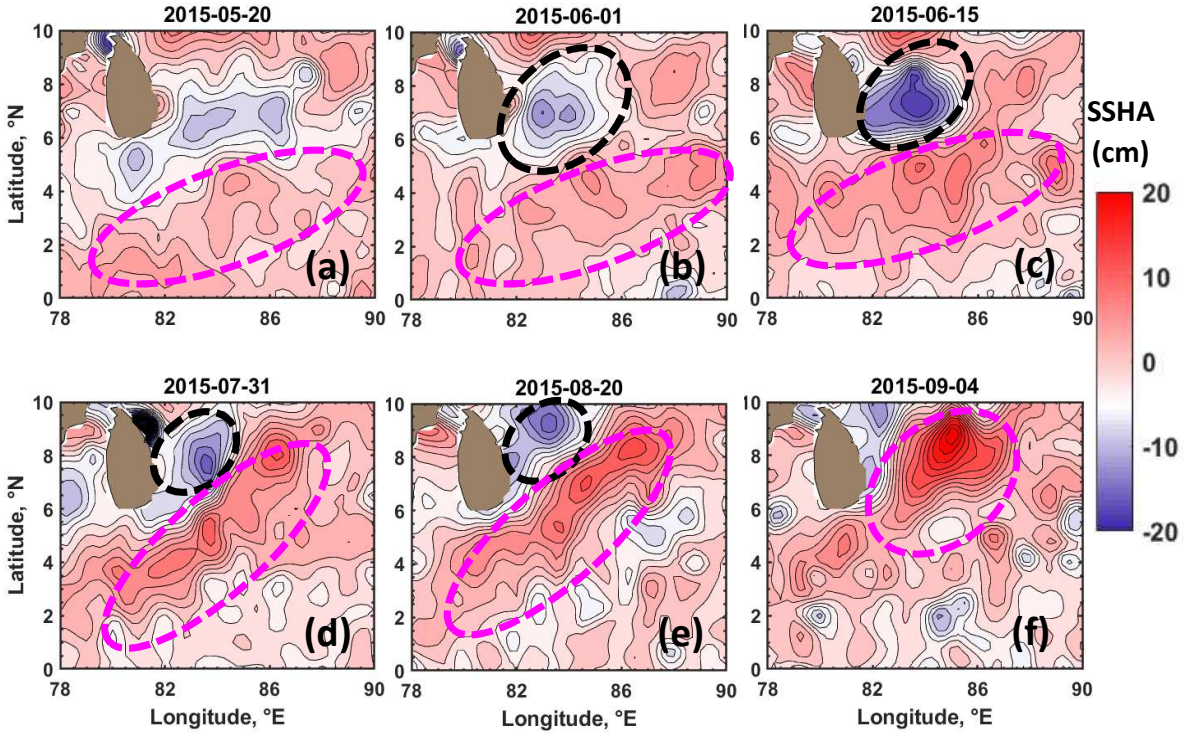

Fig. 8: AVISO SSHA maps. Evolution of SLD (black broken line) in conjunction with the AE (magenta dashed line) from May to September 2015.

6. *Laboratory experimental results*

Laboratory observations with approximately matched π and Ro between the SMC and the laboratory jet are shown in Fig. 11a. The (yellow) particle tracks have been retrieved using the

633 Particle Tracking Velocimetry (PTV) based on a frame record of ~ 30 seconds (i.e. 600 frames,
634 approximately over one rotational period following the appearance of eddies). Note the
635 anticlockwise rotation (Ω) of the laboratory tank. The topographically-perturbed eastward flow
636 on the β plane (green arrow) develops a negative vorticity due to potential vorticity conservation,
637 leading to the AE. A cyclonic eddy (SLD) is formed simultaneously, the growth of which is
638 affected by the Sri Lanka topography. Upon formation, the laboratory eddies are influenced by
639 the local Coriolis effects. While other less-pronounced eddies associated with or triggered by the
640 trapped Rossby wave appear in BoB, as marked by drifter tracks (Fig. 7a), such multiple eddies
641 are absent in the laboratory possibly because of weak jet forcing at the exit and the bottom
642 friction. The theoretical diameter of the laboratory anticyclonic eddy $\pi(U_0/\beta)^{1/2}$ ranges
643 between 10 and 18 cm, and the observed laboratory values are between 12 and 19 cm (estimated
644 as the distance from the eddy center to the streamline of maximum velocity). The corresponding
645 theoretical AE diameter in BoB is ~ 500 km (Section 2), which was close to the observations
646 (Section 4.1). The velocity of the laboratory anti-cyclonic eddy from the PTV analysis was
647 between 0.11 and 0.34 cm s^{-1}, and based on π similarity this corresponds to an AE oceanic
648 velocity of ~ 0.7 – 0.8 m s^{-1}, which is comparable to what observed during ADCP observations
649 (Sections 4.1 and 4.2).

650 The difficulty of detailed comparisons between laboratory and ocean observations should
651 be emphasized here, given the myriad processes, planetary waves and their interactions present
652 in the ocean that add to the complexity. For example, the location of the laboratory AE was
653 farther south of that observed in the ocean. The aim of the laboratory experiment, however, was
654 to demonstrate the possibility of AE and SLD as a result of trapped Rossby waves (i.e. β effect
655 and topography) in support of the hypothesis advanced before.

656 The same experiment was conducted without the Sri Lanka model, and the results are
657 shown in Fig. 11b. Without the topographic perturbation, the cyclonic/anticyclonic eddy pair
658 (originating from the trapped Rossby-wave) is absent, and the flow simply deflects due to the
659 Coriolis effect and forms a single eddy with a diameter varying between 15 and 21 cm. Eddy
660 velocity remain still within 0.11 and 0.34 cm s^{-1}.

661 Another controlled experiment was conducted without the simulated β effect (i.e. with a
662 flat bottom, $\alpha = 0$), but with otherwise identical forcing parameters to the previous cases (Fig.
663 12c). The flow separation generated some cyclonic vorticity but velocities within the eddy were
664 significantly smaller than that in the anticyclonic eddy formed by Coriolis deflection of the jet.
665 On this *f* plane (i.e. $\beta = 0$ case) the AE is somewhat smaller and displaced to farther south of the
666 island compared to Fig. 11a, arguably due to the lack of a Rossby wave response. Voropayev et
667 al. (1997) have studied jets on a *f* plane, and proposed an anticyclonic eddy diameter scale ~
668 U_0/f_0. Accordingly, our *f* plane experiments ought to produce an AE of diameter ~ 5.2 cm, and
669 the observed eddy diameter was ~ 7 cm.

670 The sensitivity to the shape of the coast was also considered in a set of experiments. In
671 particular, the island was shaped with a cylinder and a parallelepiped. For the same values of
672 bottom slope, flow velocity and tank rotation, the formation of an elliptical anticyclonic eddy
673 was observed southeast of model topography irrespective of the obstacle shape (not shown here),
674 suggesting that indeed the island is a topographic perturbation for planetary-wave genesis.
675 However, the velocity magnitude and location of eddies appear to depend on the details of the
676 topography.

677

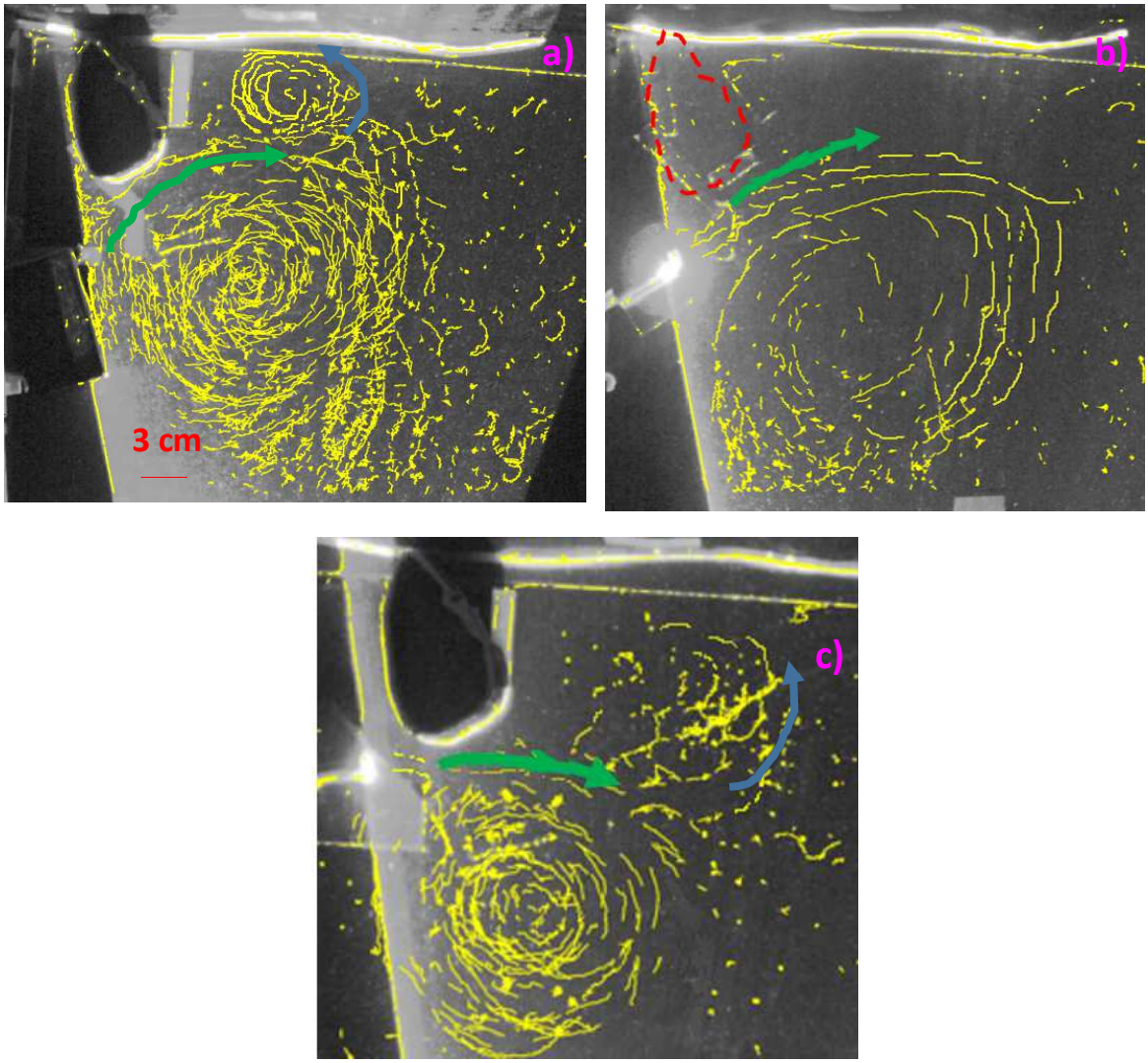

678

679

680 *Fig. 9: Laboratory experimental results illustrated using particle tracks that follow the flow. (a) For the*
681 *case of β plane (α ~ 2.3° - 2.5°), southwesterly flow in a rotating tank splits into an AE southeast of Sri*
Lanka, and a cyclonic (SLD) eddy east of Sri Lanka; (b) For flow in β plane (α ~ 2.3° - 2.5°) with no Sri
682 *Lanka, an elliptical AE is formed, triggered by the southwesterly flow. Red dashed line indicates that Sri*
Lanka was removed. (c) For the f plane case (α=0), southwesterly flow splits into a smaller circular AE
683 *south of Sri Lanka, and a weaker cyclonic eddy east of the island, indicating that the flow separation is*
insufficient to produce a strong cyclonic eddy. Green (blue) arrows indicate AE (SLD) flow direction.

684

685

7. Summary and discussion

This paper concerned the nature and dynamics of eddies and currents in the southwestern Bay of Bengal (BoB), specifically the Sri Lanka Dome (SLD), the Anticyclonic Eddy (AE) and the Southwest Monsoon Current (SMC). It synthesizes observations from two recent cruises (2015, 2018), satellite platforms, numerical simulations and a laboratory experiment to confirm the recurring nature of the eddies, identify their characteristics as well as the generation and evolution mechanisms. The main results are:

(i) A simple theoretical analysis suggests that a trapped Rossby wave response of the SMC may produce broad eddy features of the southwestern BoB, and barotropic instability of these waves lead to the SLD and AE forming on either side of the meandering SMC. This notion is supported by animated satellite imagery and COAMPS® regional simulations that indicate both eddies are formed almost simultaneously with the genesis of the SMC in the early summer. These results are at odds with the previous proposal of Vinayachandran and Yamagata (1998) for AE formation, that is, collision between the SMC and southeasterly Rossby waves generated off the coast of Sumatra due to impingement of the spring Wyrtki jet may be the cause for the AE. Our observations as well as model simulations show that such waves do not arrive in the southwestern BoB until late summer (August/September) whereas the SLD and AE appear soon after the SMC is formed. De Vos et al. (2014) suggest that the SLD is formed due to the separation of the SMC from the southern cost of Sri Lanka, but this mechanism cannot account for the simultaneous AE formation as observed, which requires anticyclonic vorticity generation. It is worth noting that Boyer and Davies (1982) and Merkine (1980) have shown that separation of an eastward jet from a topography on β plane is inhibited when $Ek^{1/2} < Ro(H/L)$, where H

709 is the depth of flow and L the horizontal scale, Ro the Rossby number and Ek the Ekman
710 number. For the SMC, $Ek^{1/2}$ = 2.6 x 10^{-6} and $R_o(H/R)$= 7 x 10^{-3}, and thus the flow separation
711 is assumed to be minor.

712 It is worth noting that Pirro et al. (this issue) estimated the eddy kinetic energy production
713 term $-<u'v'>dU_0/dz$ using the mooring data of Wijesekera et al. (2016a). The production
714 term was positive in the upper 100 m for the time period where the AE was present in August
715 2014, suggesting that the SMC may undergo barotropic instability and transfers kinetic energy
716 from the main flow to AE and SLD.

717 (ii) Considering all evidence, we argue that Rossby wave dynamics is the main cause for
718 the SLD and the AE. The predicted half wavelength of the Rossby wave $\lambda=\pi(\overline{U}_o/\beta)^{1/2}$ ~ 500
719 km matched the distance where the AE appears downstream of Sri Lanka, further supporting our
720 hypothesis. Barotropic Rossby waves are inherently unstable and generate cyclonic (SLD) and
721 anticyclonic eddies on either side of the jet (SMC). Barotropic instability of a zonal jet on the
722 f plane without the β effect also produces instabilities, but the estimated wave length is too large
723 to be reconciled with the observations.

724 (iii) An exploratory laboratory experiment with dynamic similitude between the SMC and
725 laboratory for the initial flow development period further supports the proposed eddy formation
726 mechanism. In the presence of the β effect, the development of the AE together with somewhat
727 smaller cyclonic eddy (SLD) to the north was observed in the laboratory. An identical
728 experiment but without the β effect produced an anticyclonic eddy only, accompanied by a weak
729 cyclonic eddy due to flow separation by the Sri Lanka model. By removing Sri Lanka landmass
730 while retaining the β effect, the cyclonic eddy disappeared altogether and only the Coriolis
731 deflection of the jet was observed. Overall, laboratory results indicate that the SMC on β plane

732 may excite topographically trapped unstable Rossby waves, producing eddy structures similar to
733 those observed in the southwestern BoB.

734 (iv) During the 2015 summer cruise, ADCP current vectors recorded a velocity of ~ 1 m s^{-1}
735 in the AE, which penetrated to the thermocline depth of ~ 150 m. AVISO SSHA satellite data
736 averaged over the cruise period (August 1st - 15th 2015) confirmed the AE with positive SSHA of
737 about 5 - 10 cm. Trajectories of drifters followed the SMC and segments of eddies. The SLD was
738 clearly evident in the negative SSHA data. Satellite SST maps indicate that colder water
739 advected by the SMC occupies a good fraction of the AE surface water (temperature ~ 28.6°C)
740 while the nearby SLD reaching SST as high as 29.6°C. Upwelling in the southern Sri Lanka and
741 Indian coasts is the source of the colder water. Observations in 2018 summer was similar, with
742 SST in the AE (~ 28.5°C) and the SLD (~ 30°C). The lower latent and sensible heats in the AE
743 measured by the ship's flux tower indicate that transport of upwelled colder water from the south
744 of Sri Lanka by the SMC may have implications on air-sea fluxes in the southwestern BoB.

745

746

747 **Acknowledgements**

748

749 We are grateful to the crew of R/V Roger Revelle and R/V Thomas G. Thompson, and a
750 group of University of Notre Dame and Naval Research Laboratory (NRL) scientists and
751 technical personnel for assistance with shipboard instrumentations. We are grateful to the
752 National Aquatic Resource Research and Development Agency (NARA) scientists for their help.
753 ASIRI and MISO-BoB projects were funded by the US Office of Naval Research (ONR) and
754 NRL. The University of Notre Dame group gratefully acknowledge the support through ONR
755 grant #N00014-17-1-2334. The paper was considerably improved while responding to two
756 thoughtful referees, and we wish to sincerely thank them.

757

758 **References**

759

760 Alaee, M.J., Ivey, G. and Pattiaratchi, C., 2004. Secondary circulation induced by flow curvature
761 and Coriolis effects around headlands and islands. Ocean Dynamics, 54(1), 27-38.

762 Batchelor, G. K., 1967: An Introduction to Fluid Dynamics, Cambridge Univ. Press, Cambridge,
763 U. K.

764 Boyer, D. L., and P. A. Davies, 1982. Flow past a circular cylinder on a β-plane. Philosopical
765 Transactions Royal Society of London A 306.1496: 533-556.

766 Centurioni, Luca R. 2018. Drifter Technology and Impacts for Sea Surface Temperature, Sea-
767 Level Pressure, and Ocean Circulation Studies. in R. Venkatesan, Amit Tandon, Eric

768 D'Asaro and M. A. Atmanand (eds.), Observing the Oceans in Real Time (Springer
769 International Publishing: Cham).
770 Das, U., Vinayachandran, P.N. and Behara, A., 2016. Formation of the southern Bay of Bengal
771 cold pool. Climate Dynamics, 47(5-6), 2009-2023. https://doi.org/10.1007 /s00382-015-
772 2947-9
773 De Vos, A.D., Pattiaratchi, C.B. and Wijeratne, E.M.S., 2014. Surface circulation and upwelling
774 patterns around Sri Lanka. Biogeosciences, 11(20), 5909-5930.
775 Durand, F., Shankar, D., Birol, F. and Shenoi, S.S.C., 2009. Spatiotemporal structure of the East
776 India Coastal Current from satellite altimetry. Journal of Geophysical Research:
777 Oceans, 114(C2). http://dx.doi.org/10.1029/2008JC004807.
778 Gill, A.E., 1974. The stability of planetary waves on an infinite beta-plane. Geophysical and
779 Astrophysical Fluid Dynamics, 6(1), 29-47.
780 Gill, A.E., 1982. Atmosphere-Ocean Dynamics, Academic Press.
781 Greatbatch, Richard J., 1985. Kelvin wave fronts, Rossby solitary waves and the nonlinear spin-
782 up of the equatorial oceans. Journal of Geophysical Research: Oceans **90.C5**: 9097-9107.
783 Hastenrath S. and Greiscahr L., 1991. The monsoonal current regimes of the tropical Indian
784 Ocean: Observed surface flow fields and their geostrophic and wind-driven
785 components. Journal of Geophysical Research: Oceans **96.C7**: 12619-12633.
786 Hocut, C.M., Liberzon, D. and Fernando, H.J.S., 2015. Separation of upslope flow over a
787 uniform slope. Journal of Fluid Mechanics, 775, 266-287.
788 Jensen, T.G., 2001. Arabian Sea and Bay of Bengal exchange of salt and tracers in an ocean
789 model. Geophysical Research Letters **28(20)**: 3,967–3,970,
790 http://dx.doi.org/10.1029/2001GL013422.

791 Jensen, T.G., 2003. Cross-equatorial pathways of salt and tracers from the northern Indian
792 Ocean: Modelling results. Deep Sea Research Part II **50(12–13)**: 2,111–2,127.
793 http://dx.doi.org/10.1016/ S0967-0645(03)00048-1.
794 Jensen, T.G., Shinoda, T., Chen, S. and Flatau, M., 2015. Ocean response to CINDY/DYNAMO
795 MJOs in air-sea-coupled COAMPS. Journal of the Meteorological Society of Japan. Ser.
796 II, 93, 157-178.
797 Jensen, T. G., Wijesekera, H. W., Nyadjro, E. S., Thoppil, P. G., Shriver, J. F., Sandeep, K. K.,
798 & Pant, V., 2016. Modeling salinity exchanges between the equatorial Indian Ocean and
799 the Bay of Bengal. Oceanography, 29(2), 92-101.
800 Killworth, P.D., 1980. Barotropic and baroclinic instability in rotating stratified fluids. Dynamics
801 of Atmospheres and Oceans, 4(3),143-184.
802 Lozovatsky, I., Wijesekera, H., Jarosz, E., Lilover, M.J., Pirro, A., Silver, Z., Centurioni, L. and
803 Fernando, H.J.S., 2016. A snapshot of internal waves and hydrodynamic instabilities in
804 the southern Bay of Bengal. Journal of Geophysical Research: Oceans, 121(8), 5898-
805 5915.
806 Mahadevan, A., Paluszkiewicz, T., Ravichandran, M., Sengupta, D. and Tandon, A., 2016.
807 Introduction to the special issue on the Bay of Bengal: From monsoons to
808 mixing. Oceanography, 29(2), 14-17.
809 McCreary Jr, J.P., Kundu, P.K. and Molinari, R.L., 1993. A numerical investigation of dynamics,
810 thermodynamics and mixed-layer processes in the Indian Ocean. Progress in
811 Oceanography, 31(3), 181-244.

McCreary, J.P., Han, W., Shankar, D. and Shetye, S.R., 1996. Dynamics of the east India coastal current: 2. Numerical solutions. Journal of Geophysical Research: Oceans, 101(C6), 13993-14010.

Merkine, Lee-Or, 1980: Flow separation on a beta plane. Journal of Fluid Mechanics. 99.2, 399-409.

Mukherjee, A., Shankar, D., Fernando, V., Amol, P., Aparna, S.G., Fernandes, R., Michael, G.S., Khalap, S.T., Satelkar, N.P., Agarvadekar, Y. and Gaonkar, M.G., 2014. Observed seasonal and intraseasonal variability of the East India Coastal Current on the continental slope. Journal of earth system science, 123(6), pp.1197-1232. http://dx.doi.org/10.1007/s12040-014-0471-7.

Murty, V.S.N., Sarma, Y.V.B., Rao, D.P. and Murty, C.S., 1992. Water characteristics, mixing and circulation in the Bay of Bengal during southwest monsoon. Journal of Marine Research, 50(2), 207-228.

Niiler PP, Sybrandy A, Bi K, Poulain PM, Bitterman D, 1995. Measurements of the water-following capability of holey-sock and TRISTAR drifters. Deep-Sea Res 1(42):1951–1964.

Pirro, A., Wijesekera, H.W., Jarosz, E., Fernando, H.J.S., 2019. Dynamics of Intra-seasonal Oscillations in Bay of Bengal during Summer Monsoons Captured by Mooring Observations, Deep Sea Research II, this issue.

Potemra, J.T., Luther, M.E. and O'Brien, J.J., 1991. The seasonal circulation of the upper ocean in the Bay of Bengal. Journal of Geophysical Research: Oceans, 96(C7), 12667-12683.

Rao, T.S. and Griffiths, R.C., 1998. Understanding the Indian Ocean: perspectives on oceanography, UNESCO publishing Paris.

835 Shankar, D., Vinayachandran, P.N. and Unnikrishnan, A.S., 2002. The monsoon currents in the
836 north Indian Ocean. Progress in oceanography, 52(1), 63-120.
837 Shetye, S.R., Gouveia, A.D., Shenoi, S.S.C., Sundar, D., Michael, G.S., Almeida, A.M. and
838 Santanam, K., 1990. Hydrography and circulation off the west coast of India during the
839 southwest monsoon 1987. Journal of Marine Research, 48(2), 359-378.
840 Shetye, S.R., Gouveia, A.D., Shankar, D., Shenoi, S.S.C., Vinayachandran, P.N., Sundar, D.,
841 Michael, G.S. and Nampoothiri, G., 1996. Hydrography and circulation in the western
842 Bay of Bengal during the northeast monsoon. Journal of Geophysical Research:
843 Oceans, 101(C6), 14011-14025. http://dx.doi.org/ 10.1029/95JC03307.
844 Schott, F., Reppin, J., Fischer, J. and Quadfasel, D., 1994. Currents and transports of the
845 Monsoon Current south of Sri Lanka. Journal of Geophysical Research: Oceans, 99(C12),
846 25127-25141.
847 Schott, F. A., and J. P. McCreary, 2001. The monsoon circulation of the Indian Ocean. Progress
848 in Oceanography, **51.1**: 1-123.
849 Tomczak, M. and Godfrey, J., 2003. Regional Oceanography: An introduction. 2nd Edition,
850 Elsevier.
851 Vinayachandran, P.N., Shetye, S.R., Sengupta, D. and Gadgil, S., 1996. Forcing mechanisms of
852 the Bay of Bengal. Curr. Sci, 70(10), 753-763.
853 Vinayachandran, P. N., and T. Yamagata, 1998. Monsoon response of the sea around Sri Lanka:
854 Generation of thermal domes and anticyclonic vortices. Journal of Physical
855 Oceanography, **28**, 1946-1960.

856 Vinayachandran, P.N., Masumoto, Y., Mikawa, T. and Yamagata, T., 1999. Intrusion of the
857 southwest monsoon current into the Bay of Bengal. Journal of Geophysical Research:
858 Oceans, 104(C5), 11077-11085. http://dx.doi.org/10.1029/1999JC900035.
859 Vinayachandran, P.N., Chauhan, P., Mohan, M. and Nayak, S., 2004. Biological response of the
860 sea around Sri Lanka to summer monsoon. Geophysical Research Letters, 31(1).
861 Vinayachandran, P.N., Shankar, D., Vernekar, S., Sandeep, K.K., Amol, P., Neema, C.P. and
862 Chatterjee, A., 2013. A summer monsoon pump to keep the Bay of Bengal
863 salty. Geophysical Research Letters, 40(9), pp.1777-1782. http://dx.doi.org/
864 10.1002/grl.50274.
865 Vinayachandran, P.N., Matthews, A.J., Vijay Kumar, K., Sanchez-Franks, A., Thushara, V.,
866 George, J., Vijith, V., Webber, B.G., Queste, B.Y., Roy, R. and Sarkar, A., 2018.
867 BoBBLE (Bay of Bengal Boundary Layer Experiment): Ocean–atmosphere interaction
868 and its impact on the South Asian monsoon. Bulletin of the American Meteorological
869 Society 2018.
870 Voropayev, S.I., Zhang, X., Boyer, D.L., Fernando, H.J. and Chi Wu, P., 1997. Horizontal jets in
871 a rotating stratified fluid. Physics of Fluids, 9(1), 115-126.
872 Webber, B.G., Matthews, A.J., Vinayachandran, P.N., Neema, C.P., Sanchez-Franks, A., Vijith,
873 V., Amol, P. and Baranowski, D.B., 2018. The dynamics of the Southwest Monsoon
874 current in 2016 from high-resolution in situ observations and models. Journal of Physical
875 Oceanography, 48(10), 2259-2282.
876 Wijesekera, H.W., Jensen, T.G., Jarosz, E., Teague, W.J., Metzger, E.J., Wang, D.W., Jinadasa,
877 S.U.P., Arulananthan, K., Centurioni, L.R. and Fernando, H.J.S., 2015. Southern Bay of

878 Bengal currents and salinity intrusions during the northeast monsoon. Journal of
879 Geophysical Research: Oceans, 120(10), 6897-6913.
880 Wijesekera, H.W., Teague, W.J., Wang, D.W., Jarosz, E., Jensen, T.G., Jinadasa, S.U.P.,
881 Fernando, H.J.S. and Hallock, Z.R., 2016a. Low-frequency currents from deep moorings
882 in the Southern Bay of Bengal. Journal of Physical Oceanography, 46(10), 3209-3238.
883 http://dx.doi.org/10.1175/JPO-D-16-0113.1.
884 Wijesekera, H.W., Shroyer, E., Tandon, A., Ravichandran, M., Sengupta, D., Jinadasa, S.U.P.,
885 Fernando, H.J., Agrawal, N., Arulananthan, K., Bhat, G.S. and Baumgartner, M., 2016b.
886 ASIRI: An ocean–atmosphere initiative for Bay of Bengal. Bulletin of the American
887 Meteorological Society, 97(10), 1859-1884.
888 Wyrtki, Klaus, 1973. An equatorial jet in the Indian Ocean. Science **181.4096**: 262-264.
889 Yu, L., O'Brien, J.J. and Yang, J., 1991. On the remote forcing of the circulation in the Bay of
890 Bengal. Journal of Geophysical Research: Oceans, 96(C11), 20449-20454.
891
892